Geochemistry Geophysics Geosystems G3
AN ELECTRONIC JOURNAL OF THE EARTH SCIENCES
Published by AGU and the Geochemical Society

Article
Volume 10, Number 1
29 January 2009
Q01Y04, doi:10.1029/2008GC002276
ISSN: 1525-2027

Low-temperature magnetic properties of greigite (Fe_3S_4)

Liao Chang and Andrew P. Roberts
National Oceanography Centre, University of Southampton, European Way, Southampton SO14 3ZH, UK (chang1@noc.soton.ac.uk)

Christopher J. Rowan
National Oceanography Centre, University of Southampton, European Way, Southampton SO14 3ZH, UK

Now at School of Geosciences, University of Edinburgh, Grant Institute, The King's Buildings, West Mains Road, Edinburgh EH9 3JW, UK

Yan Tang
Hefei National Laboratory for Physical Sciences at Microscale and Department of Materials Science and Engineering, University of Science and Technology of China, Hefei 230026, China

Now at College of Chemical Engineering and Technology, Wuhan University of Science and Technology, Wuhan 430081, China

Petr Pruner
Institute of Geology AS CR, v.v.i., Rozvojová 269, CZ-16500 Prague, Czech Republic

Qianwang Chen
Hefei National Laboratory for Physical Sciences at Microscale and Department of Materials Science and Engineering, University of Science and Technology of China, Hefei 230026, China

Chorng-Shern Horng
Institute of Earth Sciences, Academia Sinica, P.O. Box 1–55, Nankang, Taipei 115, Taiwan

[1] We provide comprehensive low-temperature magnetic results for greigite (Fe_3S_4) across the spectrum from superparamagnetic (SP) to multidomain (MD) behavior. It is well known that greigite has no low-temperature magnetic transitions, but we also document that it has strong domain-state dependence of magnetic properties at low temperatures. Blocking of SP grains and increasing thermal stability with decreasing temperature is apparent in many magnetic measurements. Thermally stable single-domain greigite undergoes little change in magnetic properties below room temperature. For pseudo-single-domain (PSD)/MD greigite, hysteresis properties and first-order reversal curve diagrams exhibit minor changes at low temperatures, while remanence continuously demagnetizes because of progressive domain wall unpinning. The low-temperature demagnetization is grain size dependent for PSD/MD greigite, with coarser grains undergoing larger remanence loss. AC susceptibility measurements indicate consistent blocking temperatures (T_B) for all synthetic and natural greigite samples, which are probably associated with surficial oxidation. Low-temperature magnetic analysis provides much more information about magnetic mineralogy and domain state than room temperature measurements and enables discrimination of individual components within mixed magnetic mineral assemblages. Low-temperature rock magnetometry is therefore a useful tool for studying magnetic mineralogy and granulometry of greigite-bearing sediments.

Components: 6868 words, 6 figures.

Keywords: greigite; low-temperature magnetic properties; domain state.

Index Terms: 1540 Geomagnetism and Paleomagnetism: Rock and mineral magnetism; 1512 Geomagnetism and Paleomagnetism: Environmental magnetism.

Received 9 October 2008; **Revised** 2 December 2008; **Accepted** 12 December 2008; **Published** 29 January 2009.

Chang, L., A. P. Roberts, C. J. Rowan, Y. Tang, P. Pruner, Q. Chen, and C.-S. Horng (2009), Low-temperature magnetic properties of greigite (Fe_3S_4), *Geochem. Geophys. Geosyst.*, *10*, Q01Y04, doi:10.1029/2008GC002276.

Theme: Advances in Instrumentation for Paleomagnetism and Rock Magnetism
Guest Editors: M. Fuller, B. Goodman, J. Kirschvink, and K. Verosub

1. Introduction

[2] Low-temperature (T < 300 K) rock magnetometry is widely used in rock magnetism and environmental magnetism [e.g., *Dunlop and Özdemir*, 1997; *Moskowitz et al.*, 1998] for magnetic mineral identification, magnetic granulometry, quantification of superparamagnetism in ultra-fine-grained nanophases, and detection of magnetic ordering and phase transitions. Low-temperature magnetic measurements involve thermal dynamic processes, which provide much more information about magnetic systems than room temperature analysis alone. Compared with high-temperature (T > 300 K) measurements, low-temperature methods also avoid chemical alteration.

[3] The low-temperature magnetic properties of magnetite (Fe_3O_4) have been extensively studied because of its importance as a terrestrial magnetic mineral and because it undergoes the Verwey transition (a crystallographic change from a cubic to a monoclinic superstructure) at ~120 K and the magnetic isotropic point (where the magnetocrystalline anisotropy constant K_1 is zero and changes sign) at 130 K. In contrast, the magnetic behavior of the thiospinel counterpart of magnetite, greigite (Fe_3S_4), which forms in sulfate-reducing sedimentary systems [e.g., *Berner*, 1984], is less well known because it was generally considered to be metastable over geological timescales and therefore rare in natural systems. However, greigite has now been widely identified in marine and lake sedimentary sequences [e.g., *Snowball and Thompson*, 1988, 1990; *Krs et al.*, 1990, 1992; *Tric et al.*, 1991; *Horng et al.*, 1992; *Roberts and Turner*, 1993; *Reynolds et al.*, 1994; *Florindo and Sagnotti*, 1995; *Housen and Musgrave*, 1996; *Roberts et al.*, 1996; *Horng et al.*, 1998; *Sagnotti and Winkler*, 1999; *Liu et al.*, 2004; *Rowan and Roberts*, 2006; *Babinszki et al.*, 2007; *Florindo et al.*, 2007; *Frank et al.*, 2007; *Ron et al.*, 2007; *Vasiliev et al.*, 2007] and it is also produced by magnetotactic bacteria in anoxic marine environments [e.g., *Mann et al.*, 1990]. Its increased recognition has made it more important to understand the magnetic properties of greigite. Published magnetic data for greigite have mostly been measured at room temperature or high temperatures, while low-temperature data for greigite consist mainly of saturation isothermal remanent magnetization (SIRM) warming curves [*Moskowitz et al.*, 1993; *Roberts*, 1995; *Roberts et al.*, 1996; *Torii et al.*, 1996; *Chang et al.*, 2007] and a few other types of low-temperature measurements, e.g., hysteresis [*Spender et al.*, 1972; *Roberts*, 1995; *Dekkers et al.*, 2000; *Chang et al.*, 2008] and FORC diagrams [*Chang et al.*, 2007]. Compared with high-temperature analysis, low-temperature analysis of greigite offers distinct advantages because of complications caused by chemical alteration at elevated temperatures [e.g., *Spender et al.*, 1972; *Krs et al.*, 1992; *Roberts*, 1995; *Dekkers et al.*, 2000; *Chang et al.*, 2008]. We present comprehensive data for a range of low-temperature measurement techniques, using greigite samples that span the grain size spectrum from superparamagnetic (SP) to multidomain (MD) behavior.

2. Samples and Methods

[4] We analyzed a range of natural and synthetic greigite samples. The natural greigite samples are from Neogene marine sediments from eastern New Zealand [*Rowan and Roberts*, 2006]; Plio-Pleistocene marine sediments from the Lower

Gutingkeng Formation, southwestern Taiwan [*Horng et al.*, 1998; *Jiang et al.*, 2001]; upper Pliocene marine sediments from the Valle Ricca section near Rome, Italy [*Florindo and Sagnotti*, 1995; *van Dongen et al.*, 2007]; and Miocene lacustrine sediments from the Czech Republic [*Krs et al.*, 1990]. The New Zealand greigite samples are from two locations on the Mahia Peninsula, North Island, New Zealand: the "NR" samples are from "Nukutaurua Road," while the "TC" samples are from "Te Waipera Cemetery" (see Figure 1 of *Rowan and Roberts* [2006]). The New Zealand samples contain mixtures of SP and Single domain (SD) greigite [*Rowan and Roberts*, 2006]. The samples from Taiwan and Italy contain typical SD greigite. The sample from the Czech Republic is a mixture of SD and MD greigite [*Roberts et al.*, 2006]. Pure synthetic greigite samples with dominantly coarse grains (labeled "S") were prepared according to the hydrothermal method of *Tang et al.* [2007] by reacting ferric chloride ($FeCl_3$) with thiourea (CH_4N_2S) and formic acid (HCOOH) at 170°C [*Chang et al.*, 2008]. The "S" samples with mean grain sizes as large as 13 μm have pseudo-single-domain (PSD)/MD behavior [*Chang et al.*, 2007]. An additional fine-grained synthetic greigite sample (SYN06) was produced by solid state transformation of mackinawite (FeS) to pyrite (FeS_2) via the intermediate greigite [*Hunger and Benning*, 2007]. This synthetic sample is dominated by (nonmagnetic) mackinawite but contains nanophase greigite particles (a few tens of nanometers across) [*Hunger and Benning*, 2007], which exhibit SP behavior at room temperature [*Roberts et al.*, 2006].

[5] Low-temperature magnetic measurements were made at the Institute for Rock Magnetism, University of Minnesota, USA. Low-temperature hysteresis loops, back-field demagnetization curves, and FORCs were measured using a Princeton Measurements Corporation vibrating sample magnetometer (VSM) with a cryostat. FORC diagrams [*Pike et al.*, 1999; *Roberts et al.*, 2000] were determined from 80 FORCs (averaging time of 200 ms, field spacing of 1.85 mT, smoothing factor of 3), using the FORCinel software [*Harrison and Feinberg*, 2008]. A Quantum Design magnetic properties measurement system (MPMS) was used for susceptibility and remanence measurements. For zero-field magnetization (ZFM) measurement, samples were cooled to 10 K in zero field. ZFM curves were recorded in a low field (2 mT) at stepwise increasing temperatures to 300 K. Samples were then cooled to 10 K in a low field (2 mT). Field-cooled magnetization (FCM) curves were measured in a low field (2 mT) during warming to room temperature. For zero-field cooled (ZFC) and field-cooled (FC) SIRM warming, samples were cooled to 10 K in either zero field or a large field (2.5 T). At 10 K, a 5 T field was applied and then switched off to impart a low-temperature SIRM. SIRM warming curves were measured during warming in zero field. For low-temperature cycling (LTC) of a room temperature SIRM, remanence was measured from room temperature to 10 K and back to room temperature in zero field. Alternating current (AC) susceptibility was measured with both the MPMS system and a Lakeshore Susceptometer. Samples were cooled in zero field to either 4 K or 20 K and then measured in a low AC field at several frequencies up to 400 K.

3. Results

3.1. Low-Temperature Hysteresis Properties

[6] Hysteresis and backfield demagnetization parameters (B_c, B_{cr}, M_{rs}/M_s, and B_{cr}/B_c, where B_c is coercivity, B_{cr} is coercivity of remanence, M_{rs} is saturation remanent magnetization, and M_s is saturation magnetization) for the studied greigite samples are variable below room temperature (Figure 1). For typical SD greigite from Taiwan and Italy, B_c and B_{cr} decrease monotonically with warming. B_{cr} values are noisy because this parameter can be difficult to measure. M_{rs}/M_s also decreases monotonically with increasing temperature but less rapidly than B_c and B_{cr}, and it always has values above 0.5 (Figure 1c). B_{cr}/B_c is stable at low temperatures for SD greigite (Figure 1d); values for the Italian greigite sample increase by only ~2% from 20 K to room temperature. Room temperature hysteresis parameters for a series of natural greigite samples [*Snowball*, 1997a, 1997b] have similar values to those of our SD greigite samples measured at 50 K. This probably indicates that the greigite samples measured by *Snowball* [1997a, 1997b] are even more thermally stable than our stable SD greigite samples.

[7] Hysteresis parameters for coarse-grained synthetic greigite samples are nearly temperature independent below room temperature (Figure 1). *Chang et al.* [2008] observed a local coercivity minimum at ~130 K for these samples, which is not visible at the scale of Figure 1a. The minimum is probably associated with domain wall reaccommodations in the PSD/MD greigite samples.

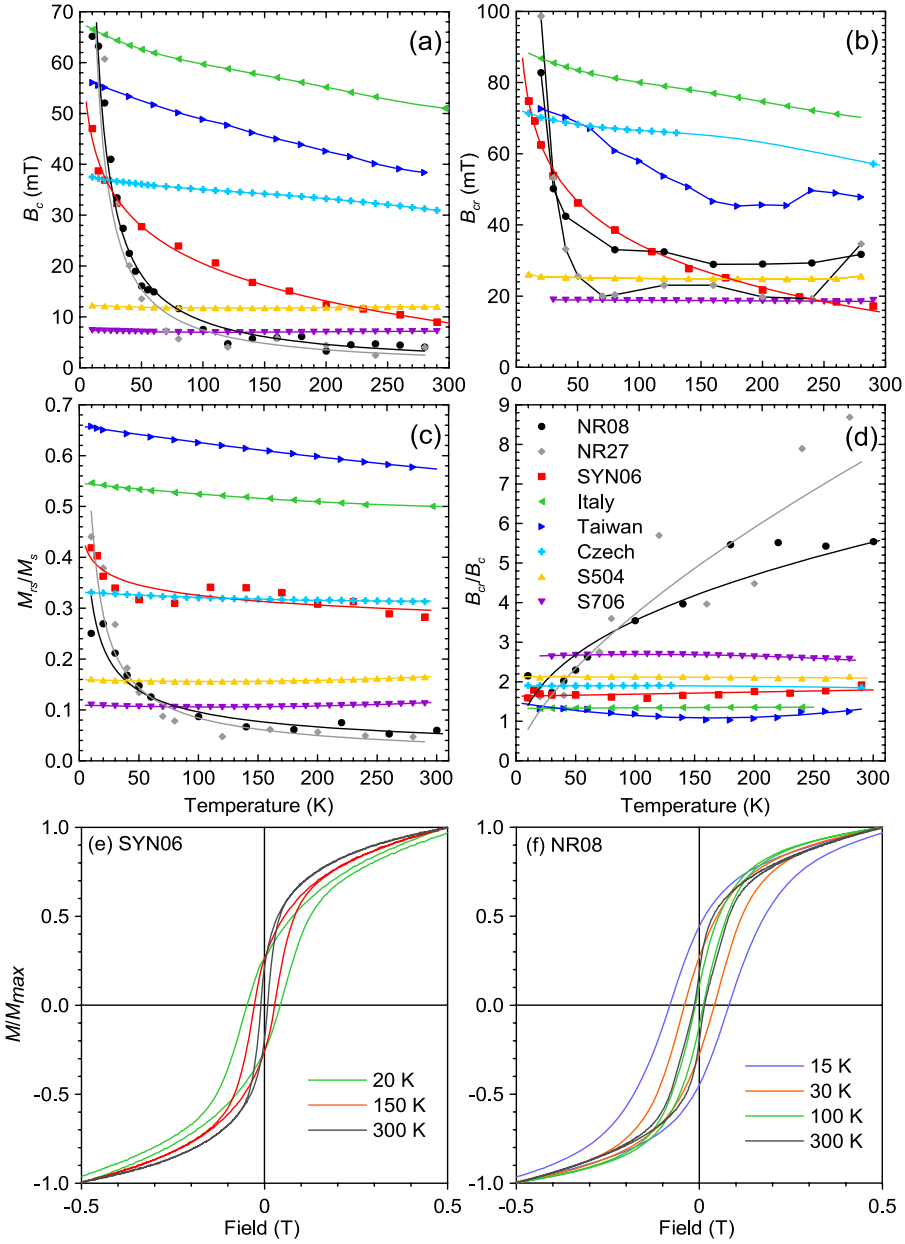

Figure 1. Temperature variations of hysteresis and back-field demagnetization properties for greigite samples below room temperature: (a) B_c, (b) B_{cr}, (c) M_{rs}/M_s, and (d) B_{cr}/B_c. Solid lines connect data points or are best fits to the data. (e, f) Low-temperature hysteresis loops for greigite-bearing samples with significant SP behavior. Fine-grained synthetic greigite sample SYN06 (Figure 1e). A magnetic separate of sample NR08 (Figure 1f). Note the broadening of the hysteresis loops as temperature decreases. The mean grain sizes for the synthetic coarse-grained samples S504 and S706 are ~4 μm and ~8 μm, respectively [cf. *Chang et al.*, 2007]. The "open" nature of the hysteresis loops at low-temperatures up to 0.5 T is probably associated with surficial oxidation.

[8] Low-temperature hysteresis properties for the fine-grained synthetic greigite sample (SYN06) indicate progressive magnetic unblocking during warming (Figure 1). B_c and B_{cr} decrease rapidly with increasing temperature (Figures 1a and 1b), which is consistent with previous reports for fine-grained synthetic greigite [e.g., *Coey et al.*, 1970; *Spender et al.*, 1972; *Dekkers et al.*, 2000]. M_{rs}/M_s and B_{cr}/B_c are noisy, but generally M_{rs}/M_s decreases, and B_{cr}/B_c increases with warming (Figures 1c and 1d). Hysteresis loops for a dominantly SP greigite sample NR08 (at room temperature, B_c = 4 mT, B_{cr} = 32 mT, M_r/M_s = 0.09) from New Zealand become broader at low temperatures

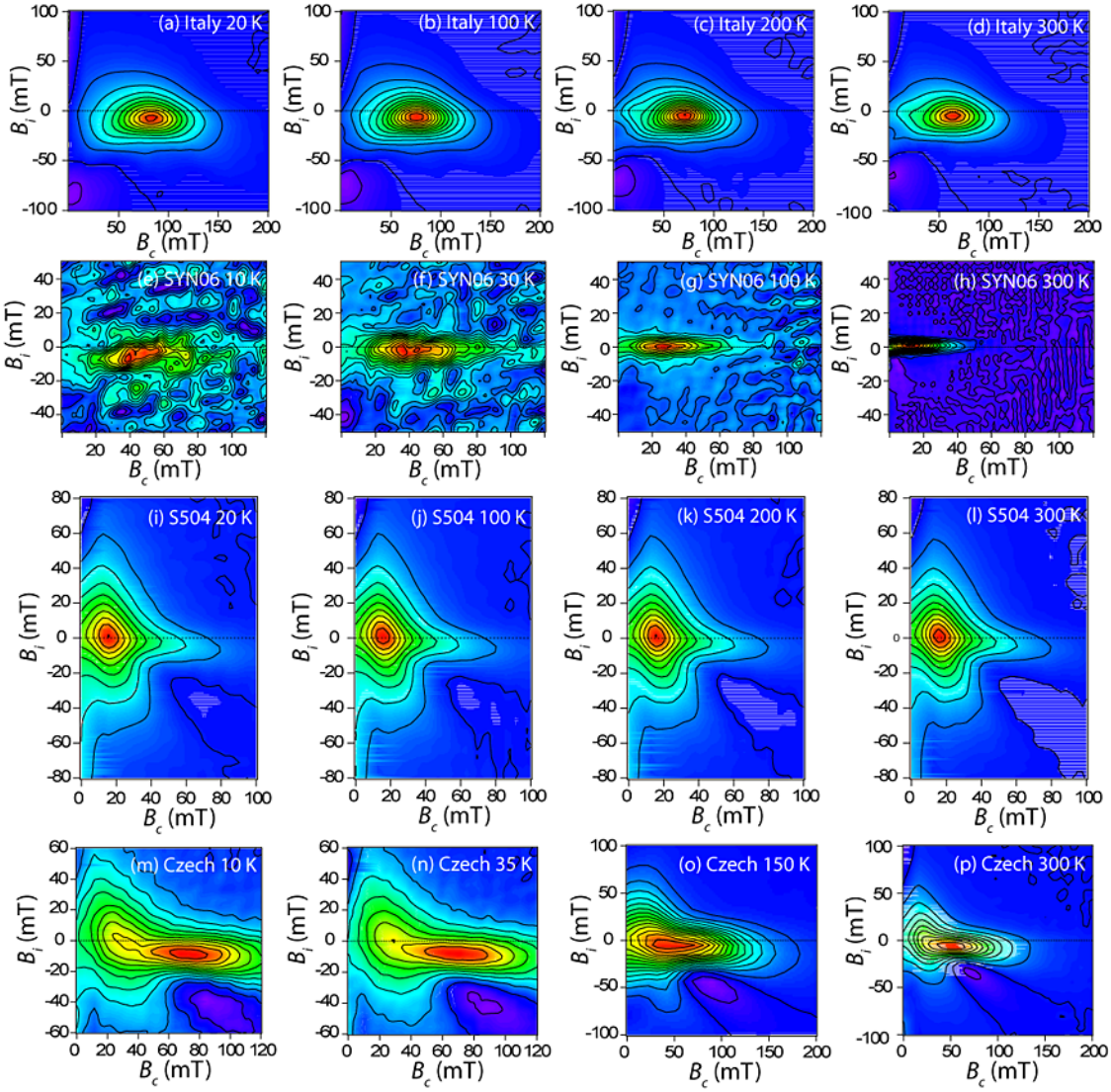

Figure 2. FORC diagrams for greigite samples at various temperatures. (a–d) A natural SD greigite sample from Italy. (e–h) Fine-grained synthetic greigite sample (SYN06) with dominantly SP behavior at room temperature. (i–l) A coarse-grained synthetic greigite sample (S504) with dominantly PSD behavior. (m–p) A natural greigite sample from the Czech Republic with a mixture of SD and PSD/MD grains. A smoothing factor (SF) [see *Roberts et al.*, 2000] of 3 was used for all FORC diagrams, except for Figures 2e and 2f for which SF = 5.

(Figure 1f), which is consistent with the behavior of sample SYN06 (Figure 1e), and indicates progressive blocking of fine magnetic particles with decreasing temperature. B_c and B_{cr} of sample NR08 decrease rapidly with warming, particularly below ~100 K (Figures 1a and 1b). M_{rs}/M_s and B_{cr}/B_c approach SD values at ~10 K (Figures 1c and 1d).

[9] Low-temperature hysteresis data for natural greigite from the Czech Republic are intermediate between those of SD and PSD/MD samples (Figure 1). B_c and B_{cr} decrease upon warming, with ~20% and ~23% decreases from 20 K to room temperature, respectively (Figures 1a and 1b). Hysteresis ratios are more stable, with only ~5% and ~3% increases for M_{rs}/M_s and B_{cr}/B_c, respectively (Figures 1c and 1d). These observations are consistent with the conclusion of *Roberts et al.* [2006] that this sample contains a mixture of SD and MD greigite.

3.2. Low-Temperature FORC Diagrams

[10] Low-temperature FORC diagrams illustrate domain-state characteristics for greigite (Figure 2). FORC distributions indicate high coercivity and strong magnetostatic interactions for natural SD

greigite [cf. *Roberts et al.*, 2000, 2006; *Rowan and Roberts*, 2006; *Florindo et al.*, 2007; *Vasiliev et al.*, 2007], without substantial low temperature variations (Figures 2a–2d). The concentric SD contours migrate toward slightly higher coercivities as temperature decreases (Figures 2a–2d), as expected for progressive blocking of a small fraction of fine particles [*Pike et al.*, 2001]. Interaction field distributions (B_i) for SD greigite undergo negligible changes at low temperatures, unlike SD magnetite [e.g., *Carvallo and Muxworthy*, 2006].

[11] Although FORC distributions for fine-grained synthetic greigite are noisy, they clearly migrate to higher coercivities at low temperatures (Figures 2e–2h), which confirms the dominantly SP behavior at room temperature for sample SYN06 [*Roberts et al.*, 2006]. This behavior is consistent with models [*Pike et al.*, 2001] and with low-temperature observations for samples with dominantly SP behavior [e.g., *Carvallo and Muxworthy*, 2006].

[12] FORC distributions for PSD/MD greigite samples are unchanged at low temperatures (Figures 2i–2l) [*Chang et al.*, 2007], as expected for MD assemblages. This contrasts with PSD magnetite, where FORC distributions split into two sets of concentric contours at low temperatures [e.g., *Carvallo and Muxworthy*, 2006; *Smirnov*, 2006]. The splitting is probably associated with induced anisotropy effects [*Smirnov*, 2006], which do not appear to be present for greigite.

[13] Low-temperature FORC diagrams for the Czech sample indicate mixed SD and PSD/MD behavior, as suggested by *Roberts et al.* [2006]. Migration of the concentric peak to higher coercivities at low temperature indicates SD behavior with minor thermal relaxation, while the divergent outer contours indicate the presence of PSD/MD grains (Figures 2m–2p).

3.3. Low-Temperature ZFM/FCM

[14] When cooled in zero magnetic field, the magnetic moments of fine particles are randomly oriented. When subsequently warmed in a weak field from low temperature, magnetic moments of the randomly oriented particles become progressively aligned with the field due to increasing thermal energy. Maximum susceptibility (where magnetic moments are maximally aligned with the field) is observed at the blocking temperature (T_B). Above T_B, susceptibility decreases as thermal energy gradually randomizes the aligned magnetic moments [*Dormann et al.*, 1997].

[15] A ZFM curve for sample SYN06 rapidly increases upon warming (Figure 3a), which indicates progressive alignment of magnetic moments with the weak field. The rapid increase over the whole temperature range probably indicates a broad grain size distribution. Although the mean T_B is above room temperature, there is significant SP behavior at room temperature. ZFM/FCM curves for some New Zealand greigite samples indicate large paramagnetic contributions, as indicated in a plot of inverse susceptibility (Figure 3b), which completely swamp ferrimagnetic greigite signals. After magnetic separation, sample NR08 has a dominant ferrimagnetic signal: the magnetization increases sharply from low temperature up to 120 K and decreases sharply from 270 K to room temperature with a broad plateau between 120 K and 270 K (Figure 3c). By removing the paramagnetic susceptibility (from hysteresis loops; insert in Figure 3d), ZFM/FCM curves can be produced that represent the ferrimagnetic signal. For sample NR27, which is dominated by SP behavior at room temperature, a peak at ~120 K in the ZFM curve (Figure 3d) indicates the mean T_B.

3.4. Low-Temperature AC Susceptibility

[16] χ (T, f) curves (where T and f are temperature and frequency, respectively) for SD greigite increase slightly during warming (Figure 4a), which suggests that the mean T_B is above room temperature. However, both the real χ' (T, f) and imaginary χ'' (T, f) components have frequency-dependent properties, which indicates the presence of some SP behavior (Figures 4a and 4d). A T_B between 6 K and 20 K is detected in the χ'' (T, f) curve (Figure 4d). Coarse-grained synthetic greigite samples undergo small susceptibility variations at low temperatures (Figure 4b), although a local susceptibility maximum was observed between 100 K and 110 K (Figure 4b). This maximum does not likely represent a T_B because it does not display frequency dependence and because it is not detected in the χ'' (T, f) curve at this temperature (Figures 4b and 4e). This local susceptibility maximum is therefore probably an intrinsic property of PSD/MD greigite. *Chang et al.* [2008] observed a local coercivity minimum for the same samples at ~130 K, but it is not clear if these properties are related. SP behavior (with a T_B between 8 K and 20 K) is indicated in the χ' (T, f) and χ'' (T, f) curves with strong frequency dependence. The observed T_B below 20 K for both synthetic and natural greigite samples (Figures 4d, 4e, and 4f) probably has a similar origin. *Chang et*

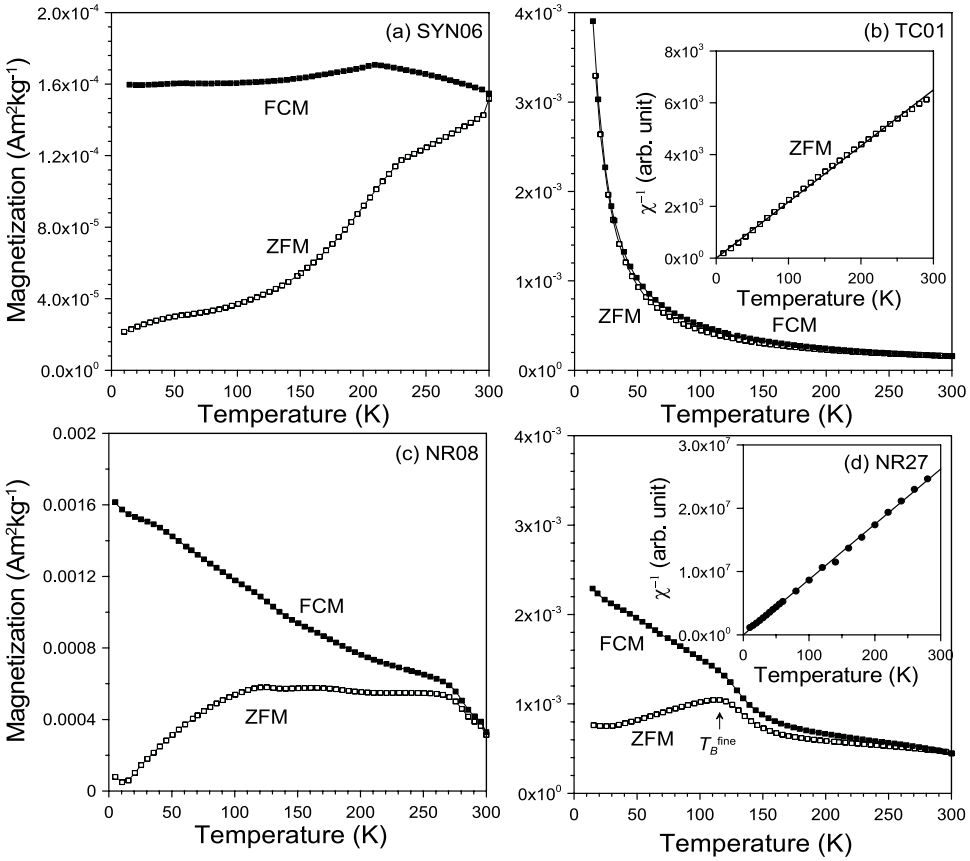

Figure 3. (a–d) ZFM/FCM curves for greigite samples in a small field (2 mT). The inserts in Figures 3b and 3d are inverse ZFM curves that indicate dominant paramagnetism across the whole temperature range. (d) ZFM/FCM curves for a greigite-bearing sediment sample from New Zealand (sample NR27) after removing the paramagnetic magnetization, which was calculated from high-field magnetization measurements (insert). See text for detailed description.

al. [2008] observed a magnetically ordered phase in synthetic greigite samples at 4 K from Mössbauer spectroscopy, which they attributed to slight surficial oxidation of greigite particles, which may be associated with the observed T_B below 20 K. This interpretation is supported by transmission electron microscope (TEM) observations of surfical oxidation on fine greigite grains [*Letard et al.*, 2005; *Kasama et al.*, 2006]. The χ' (T, f) curves for natural greigite-bearing sediments from New Zealand rapidly decrease upon warming (Figures 4g–4i), which indicates substantial paramagnetism. Weak ferrimagnetic greigite signals are often therefore swamped by paramagnetism. However, measurement of a magnetic separate (sample NR08) indicates characteristic frequency-dependent susceptibility that is associated with SP behavior (Figures 4c and 4f).

Figure 4. (a–f) The AC susceptibility for three greigite samples with SP/SD, PSD/MD, and SP properties during warming. The insert in Figure 4b is an expanded view of the main susceptibility curves. (g–i) The measured AC susceptibility (real component χ' (T, f)) for natural greigite samples from eastern New Zealand. (j–l) The inverse AC susceptibility for the same samples in Figures 4g–4i. Lines are linear fits to $\chi^{-1} = A \cdot T$ (where χ and T are susceptibility and temperature, respectively; A is a coefficient) for T < 50 K, which represent paramagnetic signals. The measured susceptibility data deviate from linearity at elevated temperatures, which indicates the increasing dominance of ferrimagnetic signals and a rapidly decreasing influence of paramagnetic susceptibility with increasing temperature. (m–o) Susceptibility curves after subtraction of the fitted paramagnetic susceptibility from the measured susceptibility for greigite samples in Figures 4g–4i. These curves represent ferrimagnetic greigite signals with variable grain size distributions. See text for detailed description. Samples in Figures 4a–4f and Figures 4g–4o were measured with a MPMS and Lakeshore Susceptometer, respectively.

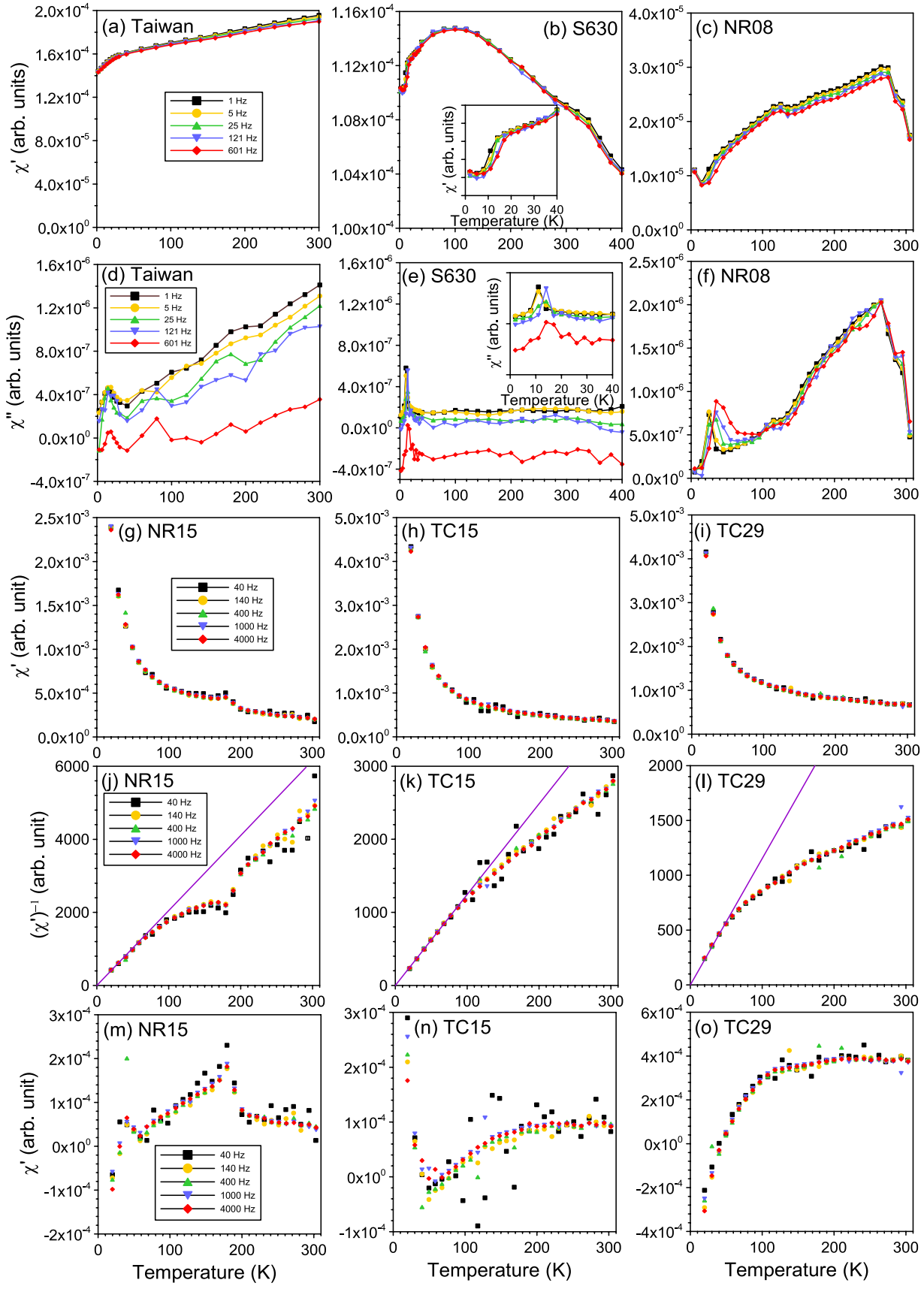
(a) Taiwan
(b) S630
(c) NR08
(d) Taiwan
(e) S630
(f) NR08
(g) NR15
(h) TC15
(i) TC29
(j) NR15
(k) TC15
(l) TC29
(m) NR15
(n) TC15
(o) TC29
1 Hz
5 Hz
25 Hz
121 Hz
601 Hz
40 Hz
140 Hz
400 Hz
1000 Hz
4000 Hz
χ' (arb. units)
χ'' (arb. units)
χ' (arb. unit)
(χ')⁻¹ (arb. unit)
Temperature (K)

Figure 4

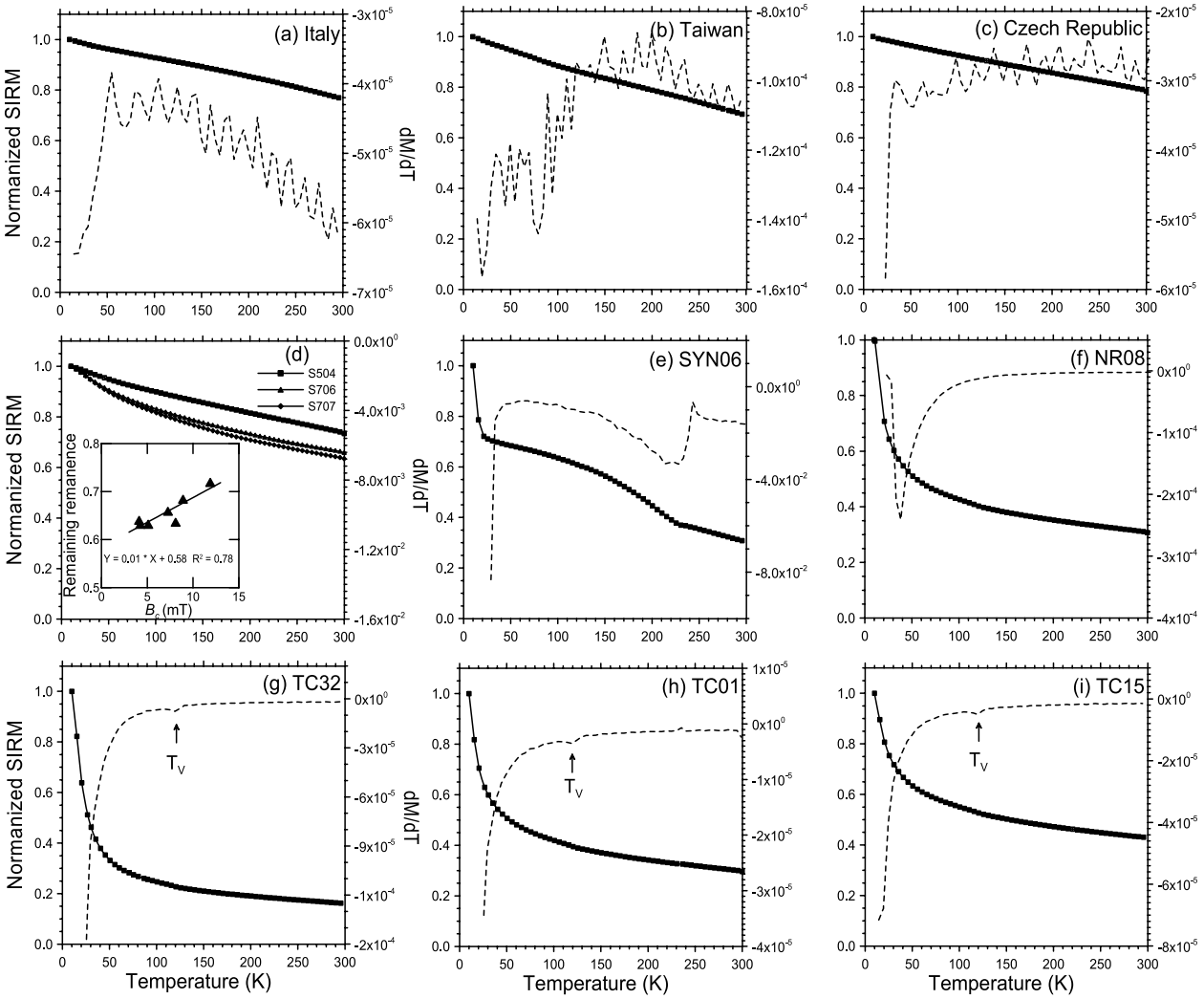

Figure 5. (a–i) SIRM warming curves for greigite samples. Solid points represent measured data. Dashed lines are the first derivative of the SIRM with respect to temperature (dM/dT). The SIRM was imparted in a 5 T field at 10 K. T_V represents the Verwey transition for magnetite. The insert in Figure 5d is the correlation between coercivity and remaining remanence after zero-field SIRM warming from 10 K to 300 K for a range of synthetic PSD/MD greigite samples.

[17] To remove the dominating effect of paramagnetic signals from matrix minerals, we linearly fitted the temperature-dependent paramagnetic AC susceptibility for T < 50 K to $1/T$ (Figures 4j–4l). We subtracted this paramagnetic susceptibility from the measured susceptibility to obtain the ferrimagnetic signal (Figures 4m–4o). Sample NR15 has a clear peak at ~180 K (Figure 4m). The imaginary component χ'' (T, f) for this sample also has peaks at this temperature, which confirms a T_B of ~180 K. For samples TC15 and TC29, the ferrimagnetic susceptibility increases rapidly up to 190 and 120 K, respectively, and is followed by nearly stable susceptibility up to room temperature (Figures 4n and 4o). These temperatures probably indicate the T_B for the SP component of the samples with a broader superposed grain size distribution that includes a stable SD component.

3.5. Low-Temperature Remanence

[18] Cooling conditions (ZFC or FC) have no effect on SIRM warming of greigite because there is no low-temperature transition for greigite [*Moskowitz et al.*, 1993; *Chang et al.*, 2007]. We therefore only show FC SIRM warming curves in Figure 5. SIRM warming curves for samples dominated by SD greigite undergo minor decreases with warming (Figures 5a and 5b), which agrees with the results of *Roberts* [1995]. SIRM decreases by 23% and 30% from 20 to 300 K for the SD

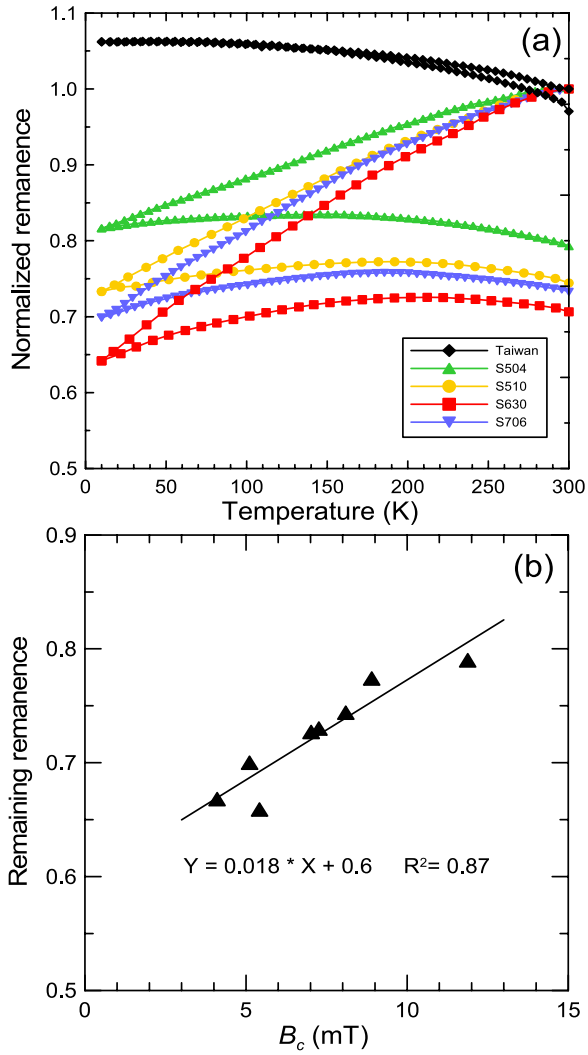

Figure 6. (a) Normalized zero-field cooling and warming of a RT-SIRM for a representative range of greigite samples that span the grain size range from SD and to PSD/MD. (b) The correlation between coercivity and remaining remanence after zero-field LTC of RT-SIRM for a range of synthetic PSD/MD greigite samples. Mean grain sizes for the synthetic coarse-grained greigite samples S504, S510, S630, and S706 are ~4 μm, ~9 μm, ~11 μm, and ~8 μm, respectively [cf. *Chang et al.*, 2007].

greigite samples from Italy and Taiwan, respectively, which indicates different SP contributions. The Czech sample has similar behavior to a previously reported sample from this locality (Figure 5c) [*Moskowitz et al.*, 1993; *Roberts*, 1995]. The SIRM for synthetic sample S706 (mean grain size of ~8 μm) decreases by 34% from 20 to 300 K (Figure 5d), which is larger than the SIRM decrease (28%) for synthetic PSD sample S504 with smaller mean grain size (<4 μm; grain sizes are reported by *Chang et al.* [2007]). Low-temperature SIRM warming curves for a range of coarse-grained synthetic greigite samples confirm that the remanence drop correlates with coercivity (insert in Figure 5d), which is a sensitive indicator of grain size for PSD/MD greigite [e.g., *Chang et al.*, 2007]. Our results therefore indicate that low-temperature SIRM warming curves are grain-size dependent for PSD/MD greigite. Coarser-grained greigite undergoes larger remanence loss during warming, although unblocking due to minor SP particles will also contribute to remanence loss.

[19] Our fine-grained synthetic greigite sample has complex SIRM warming behavior (Figure 5e). The abrupt remanence decrease from 10 to 20 K is probably due to impurities, such as an oxidized surface layer, e.g., iron oxide or hydroxide [*Letard et al.*, 2005; *Kasama et al.*, 2006]. TEM observations indicate that this sample contains extremely fine greigite grains [*Hunger and Benning*, 2007]. Therefore, surface oxidation could have a significant effect on the magnetic properties. The large remanence drop between 20 K and 230 K is likely due to unblocking of fine greigite particles. The relatively small decrease from 230 K to room temperature is probably due to an additional grain size distribution (i.e., there are bimodal and overlapping grain size distributions). The remaining remanence at room temperature is carried by SD grains, which is consistent with ZFM/FCM measurements that indicate a mixture of SP/SD grains. SIRM warming curves for the New Zealand greigite samples abruptly decrease between 20 and 300 K (Figures 5f–5i). First derivatives of SIRM warming curves indicate the presence of minor magnetite in the greigite-dominated TC samples (Figures 5g–5i), which is likely to be from detrital tuffaceous material that was not dissolved during reductive diagenesis [*Rowan and Roberts*, 2006]. Magnetite, even when present in small concentrations, can be detected by low-temperature magnetic measurements because of the effect of the Verwey transition. Regardless, trace amounts of magnetite do not significantly affect our conclusions.

[20] Finally, LTC measurements of a RT-SIRM for a natural SD greigite sample and for a range of coarse-grained synthetic samples resemble the results of *Chang et al.* [2007], which indicate contrasting behavior for SD and PSD/MD samples (Figure 6a). SP particles make no contribution to remanence, so they are not relevant to LTC of RT-SIRM measurements. For SD greigite (from Taiwan), the remanence increases slightly due to

decreased thermal energy upon cooling [*Dekkers et al.*, 2000; *Chang et al.*, 2007]. The remanence memory is nearly complete when warmed back to room temperature. In contrast, PSD/MD greigite demagnetizes during cooling and the warming curve is irreversible with respect to the cooling curve [*Chang et al.*, 2007]. Measurements on coarse-grained synthetic greigite samples indicate that the remanence memory after LTC is strongly correlated to B_c, which, in turn, is dependent on grain size (Figure 6b). LTC of a RT-SIRM therefore provides a useful tool for magnetic granulometry by enabling discrimination between SD and PSD/MD grains.

4. Discussion

[21] Comprehensive low-temperature magnetic measurements of SP to MD greigite consistently provide no evidence of a low-temperature transition. This confirms previous observations [e.g., *Coey et al.*, 1970; *Spender et al.*, 1972; *Moskowitz et al.*, 1993; *Roberts*, 1995; *Torii et al.*, 1996; *Dekkers et al.*, 2000; *Chang et al.*, 2007, 2008]. There is also no evidence for a low-temperature phase transition from structural investigations from either Mössbauer spectroscopy [*Vandenberghe et al.*, 1991; *Chang et al.*, 2008]. Greigite probably also has no low-temperature magnetic isotropic point. Low-temperature SIRM warming curves have been used to discriminate greigite from other magnetic minerals with low-temperature magnetic transitions, e.g., magnetite and pyrrhotite (Fe_7S_8) [e.g., *Moskowitz et al.*, 1993; *Roberts*, 1995; *Housen and Musgrave*, 1996; *Roberts et al.*, 1996; *Torii et al.*, 1996; *Horng et al.*, 1998; *Jiang et al.*, 2001; *Babinszki et al.*, 2007]. However, it should be noted that the absence of a magnetic transition does not enable positive identification of greigite. Additional analyses, e.g., X-ray diffraction and scanning electron microscope observations, are needed to enable unambiguous detection.

[22] At room temperature, hysteresis parameters for greigite-bearing sediments from eastern New Zealand [*Rowan and Roberts*, 2006] fall on a similar trend to SP/SD mixing lines calculated for magnetite [*Dunlop*, 2002]. Representative hysteresis loops are slightly wasp-waisted (Figure 1f) [*Rowan and Roberts*, 2006], which is consistent with the presence of SP/SD mixtures [*Roberts et al.*, 1995]. The dominantly SP greigite samples undergo the most rapid low-temperature change in magnetic properties. Low-temperature hysteresis measurements, along with ZFM/FCM and low-temperature AC susceptibility curves, also confirm the dominance of SP behavior in these sediments. Variations in the observed T_B reveal fine but variable grain size distributions. SP behavior is also present in samples dominated by SD greigite (e.g., B_c decreases by ~28% and ~44%, while SIRM decreases by 23% and 30% from 20 to 300 K for the natural greigite samples from Italy and Taiwan, respectively). These low-temperature observations are consistent with room temperature hysteresis measurements, where the Italian sample has a larger B_c value than the sample from Taiwan (50 versus 44 mT). The different decreases probably reflect different SP contributions. SP behavior in greigite-bearing sediments is unsurprising considering that greigite progressively grows from solution to a finite grain size, which favors formation of ultrafine particles [*Rowan and Roberts*, 2006]. Progressive blocking during cooling to low temperatures means that B_c, B_{cr}, and M_{rs}/M_s increase rapidly where SP behavior dominates, while B_{cr}/B_c decreases rapidly with decreasing temperature [cf. *Coey et al.*, 1970; *Spender et al.*, 1972; *Dekkers et al.*, 2000]. Concentric FORC contours move rapidly to higher coercivities. ZFM/FCM and AC susceptibility curves for dominantly SP samples have characteristic maxima that correspond to the mean T_B of the fine greigite particles. Low-temperature SIRM also decreases rapidly during warming [cf. *Roberts*, 1995; *Chang et al.*, 2007].

[23] SD greigite has relatively stable magnetic properties at low temperatures. Hysteresis parameters undergo only small changes, with slightly increasing B_c, B_{cr}, and M_{rs}/M_s and decreasing B_{cr}/B_c during cooling. FORC diagrams indicate a minor migration of the SD distribution toward higher coercivities with decreasing temperature, but these changes are much smaller than for dominantly SP samples. ZFM and AC susceptibility increases slightly during warming. SIRM decreases slightly from low to room temperature [cf. *Roberts*, 1995; *Chang et al.*, 2007]. Zero-field cycling of RT-SIRM indicates a small increase during cooling, with nearly reversible warming curves [e.g., *Chang et al.*, 2007].

[24] Temperature dependence of magnetic properties for PSD/MD greigite is mainly controlled by domain wall movements. Magnetization (hysteresis, FORC, ZFM/FCM, AC susceptibility) is usually stable, while remanence (warming, zero-field cycling) is unstable. *He et al.* [2006] observed low-temperature magnetization jumps in ZFM curves

for a synthetic greigite microrod, which they attributed to domain wall pinning effects. We did not observe such behavior, probably because of a comparatively low magnetic anisotropy for our more equant PSD/MD greigite samples [*Chang et al.*, 2008]. By contrast, the remanence is demagnetized in our samples at low temperatures as domain walls become progressively unpinned. Low-temperature demagnetization of SIRM for PSD/MD grains is associated with domain wall unpinning [e.g., *Moskowitz et al.*, 1998]. Low-temperature SIRM warming curves vary with grain size for PSD/MD greigite: coarser-grained greigite undergoes larger demagnetization. More MD-like greigite can lose significant remanence, which could be misinterpreted as SP behavior. Complementary measurements are therefore needed to resolve such ambiguities. Zero-field cycling of RT-SIRM causes significant demagnetization during cooling, and warming curves are not reversible with respect to cooling curves [*Chang et al.*, 2007]. This irreversible demagnetization is probably associated with domain reordering, i.e., domain wall reequilibration or domain nucleation due to temperature-dependent changes in magnetocrystalline anisotropy and transdomain processes [*Chang et al.*, 2007], similar to cooling processes that cause remanence decreases in PSD/MD magnetite above the Verwey transition [*Muxworthy et al.*, 2003].

5. Conclusions

[25] Greigite undergoes no low-temperature transition and it probably has no magnetic isotropic point. Low-temperature measurements indicate strong domain-state dependence of magnetic properties for greigite. SP behavior produces major changes in low-temperature measurements. SP greigite is widespread in greigite-bearing sediments, even in typical SD natural greigite samples, and can be detected despite large SD or PSD/MD background signals using SIRM warming, ZFM/FCM curves, and AC susceptibility. A T_B below 20 K was consistently observed in our greigite samples by AC susceptibility measurements, which we attribute to minor surface oxidation of greigite grains. SD greigite has relatively stable magnetic properties; coercivity increases slightly as thermally relaxed grains magnetically block at low temperature. For PSD/MD greigite, hysteresis properties, FORC diagrams, ZFM/FCM curves, and AC susceptibility are stable, while remanence demagnetizes significantly due to domain wall unpinning. MD greigite can undergo significant remanence loss during warming, which can be misinterpreted as SP behavior. Complementary measurements are therefore needed to resolve this potential ambiguity. Low-temperature magnetic measurements have the potential to unravel contributions from either mineral mixtures or mixed domain states, which provides much more information than room temperature measurements. Low-temperature rock magnetometry can therefore be widely useful for studying magnetic mineralogy and granulometry of greigite-bearing materials.

Acknowledgments

[26] Liao Chang is supported by a Dorothy Hodgkin Postgraduate Award, funded by Hutchison Whampoa Limited and the U.K. Natural Environment Research Council. We thank T. Berquó, A. Muxworthy, and Q. S. Liu for discussions and Bruce Moskowitz, Ian Snowball, and Mark Dekkers for helpful reviews of the manuscript. Funding for sampling in the Czech Republic was partly provided from the Institutional Research Plan of the GLI AS CR, v.v.i. CEZ AV0Z30130516. The Institute for Rock Magnetism, which is funded by the National Science Foundation, the Keck Foundation, and the University of Minnesota, provided two visiting fellowships that enabled the low-temperature measurements. Mike Jackson, Julie Bowles, Peat Sølheid, Brian Carter-Stiglitz, and Amy Chen helped with measurements.

References

Babinszki, E., E. Marton, P. Marton, and L. F. Kiss (2007), Widespread occurrence of greigite in the sediments of Lake Pannon: Implications for environment and magnetostratigraphy, *Palaeogeogr. Palaeoclimatol. Palaeoecol.*, *252*, 626–636, doi:10.1016/j.palaeo.2007.06.001.

Berner, R. A. (1984), Sedimentary pyrite formation: An update, *Geochim. Cosmochim. Acta*, *48*, 605–615, doi:10.1016/0016-7037(84)90089-9.

Carvallo, C., and A. R. Muxworthy (2006), Low-temperature first-order reversal curve (FORC) diagrams for synthetic and natural samples, *Geochem. Geophys. Geosyst.*, *7*, Q09003, doi:10.1029/2006GC001299.

Chang, L., A. P. Roberts, A. R. Muxworthy, Y. Tang, Q. W. Chen, C. J. Rowan, Q. S. Liu, and P. Pruner (2007), Magnetic characteristics of synthetic pseudo-single-domain and multi-domain greigite (Fe_3S4), *Geophys. Res. Lett.*, *34*, L24304, doi:10.1029/2007GL032114.

Chang, L., A. P. Roberts, Y. Tang, B. D. Rainford, A. R. Muxworthy, and Q. W. Chen (2008), Fundamental magnetic parameters from pure synthetic greigite (Fe_3S4), *J. Geophys. Res.*, *113*, B06104, doi:10.1029/2007JB005502.

Coey, J. M. D., M. R. Spender, and A. H. Morrish (1970), The magnetic structure of the spinel, Fe_3S_4, *Solid State Commun.*, *8*, 1605–1608, doi:10.1016/0038-1098(70)90473-4.

Dekkers, M. J., H. F. Passier, and M. A. A. Schoonen (2000), Magnetic properties of hydrothermally synthesized greigite-II. High- and low-temperature characteristics, *Geophys. J. Int.*, *141*, 809–819, doi:10.1046/j.1365-246x.2000.00129.x.

Dormann, J. L., D. Fiorani, and E. Tronc (1997), *Magnetic Relaxation in Fine-Particle Systems*, *Adv. Chem. Phys.*,

vol. XCVIII, edited by I. Prigogine and S. A. Rice, pp. 283–494, John Wiley, Hoboken, N. J.

Dunlop, D. J. (2002), Theory and application of the Day plot (M_{rs}/M_s versus H_{cr}/H_c): 1. Theoretical curves and tests using titanomagnetite data, *J. Geophys. Res.*, *107*(B3), 2056, doi:10.1029/2001JB000486.

Dunlop, D. J., and Ö. Özdemir (1997), *Rock Magnetism: Fundamentals and Frontiers*, 573 pp., Cambridge Univ. Press, Cambridge, U.K.

Florindo, F., and L. Sagnotti (1995), Palaeomagnetism and rock magnetism in the upper Pliocene Valle Ricca (Rome, Italy) section, *Geophys. J. Int.*, *123*, 340–354, doi:10.1111/j.1365-246X.1995.tb06858.x.

Florindo, F., D. B. Karner, F. Marra, P. R. Renne, A. P. Roberts, and R. Weaver (2007), Radioisotopic age constraints for Glacial Terminations IX and VII from aggradational sections of the Tiber River delta in Rome, Italy, *Earth Planet. Sci. Lett.*, *256*, 61–80, doi:10.1016/j.epsl.2007.01.014.

Frank, U., N. R. Nowaczyk, and J. F. W. Negendank (2007), Palaeomagnetism of greigite bearing sediments from the Dead Sea, Israel, *Geophys. J. Int.*, *168*, 904–920, doi:10.1111/j.1365-246X.2006.03263.x.

Harrison, R. J., and J. M. Feinberg (2008), FORCinel: An improved algorithm for calculating first-order reversal curve distributions using locally weighted regression smoothing, *Geochem. Geophys. Geosyst.*, *9*, Q05016, doi:10.1029/2008GC001987.

He, Z. B., S. H. Yu, X. Y. Zhou, X. G. Li, and J. F. Qu (2006), Magnetic-field-induced phase-selective synthesis of ferrosulfide microrods by a hydrothermal process: Microstructure control and magnetic properties, *Adv. Funct. Mater.*, *16*, 1105–1111, doi:10.1002/adfm.200500580.

Horng, C. S., J. C. Chen, and T. Q. Lee (1992), Variations in magnetic minerals from two Plio-Pleistocene marine-deposited sections, southwestern Taiwan, *J. Geol. Soc. Chin.*, *35*, 323–335.

Horng, C. S., M. Torii, K. S. Shea, and S. J. Kao (1998), Inconsistent magnetic polarities between greigite- and pyrrhotite/magnetite-bearing marine sediments from the Tsailiao-chi section, southwestern Taiwan, *Earth Planet. Sci. Lett.*, *164*, 467–481, doi:10.1016/S0012-821X(98)00239-8.

Housen, B. A., and R. J. Musgrave (1996), Rock-magnetic signature of gas hydrates in accretionary prism sediments, *Earth Planet. Sci. Lett.*, *139*, 509–519, doi:10.1016/0012-821X(95)00245-8.

Hunger, S., and L. G. Benning (2007), Greigite: A true intermediate on the polysulfide pathway to pyrite, *Geochem. Trans.*, *8*(1), doi:10.1186/1467-4866-8-1.

Jiang, W. T., C. S. Horng, A. P. Roberts, and D. R. Peacor (2001), Contradictory magnetic polarities in sediments and variable timing of neoformation of authigenic greigite, *Earth Planet. Sci. Lett.*, *193*, 1–12, doi:10.1016/S0012-821X(01)00497-6.

Kasama, T., M. Pósfai, R. K. K. Chong, A. P. Finlayson, P. R. Buseck, R. B. Frankel, and R. E. Dunin-Borkowski (2006), Magnetic properties, microstructure, composition, and morphology of greigite nanocrystals in magnetotactic bacteria from electron holography and tomography, *Am. Mineral.*, *91*, 1216–1229, doi:10.2138/am.2006.2227.

Krs, M., M. Krsová, P. Pruner, A. Zeman, F. Novák, and J. Jansa (1990), A petromagnetic study of Miocene rocks bearing micro-organic material and the magnetic mineral greigite (Sokolov and Cheb basins, Czechoslovakia), *Phys. Earth Planet. Inter.*, *63*, 98–112, doi:10.1016/0031-9201(90)90064-5.

Krs, M., F. Novák, M. Krsová, P. Pruner, L. Koulíková, and J. Jansa (1992), Magnetic properties and metastability of greigite-smythite mineralization in brown-coal basins of the Krusné Hory Piedmont, Bohemia, *Phys. Earth Planet. Inter.*, *70*, 273–287, doi:10.1016/0031-9201(92)90194-Z.

Letard, I., P. Sainctavit, N. Menguy, J.-P. Valet, A. Isambert, M. Dekkers, and A. Gloter (2005), Mineralogy of greigite Fe_3S_4, *Phys. Scr. T*, *115*, 489–491, doi:10.1238/Physica.Topical.115a00489.

Liu, J., R. X. Zhu, A. P. Roberts, S. Q. Li, and J. H. Chang (2004), High-resolution analysis of early diagenetic effects on magnetic minerals in post-middle-Holocene continental shelf sediments from the Korea Strait, *J. Geophys. Res.*, *109*, B03103, doi:10.1029/2003JB002813.

Mann, S., N. H. C. Sparks, R. B. Frankel, D. A. Bazylinski, and H. W. Jannasch (1990), Biomineralization of ferrimagnetic greigite (Fe_3S_4) and iron pyrite (FeS_2) in a magnetotactic bacterium, *Nature*, *343*, 258–261, doi:10.1038/343258a0.

Moskowitz, B. M., R. B. Frankel, and D. A. Bazylinski (1993), Rock magnetic criteria for the detection of biogenic magnetite, *Earth Planet. Sci. Lett.*, *120*, 283–300, doi:10.1016/0012-821X(93)90245-5.

Moskowitz, B. M., M. Jackson, and C. Kissel (1998), Low-temperature magnetic behavior of titanomagnetites, *Earth Planet. Sci. Lett.*, *157*, 141–149, doi:10.1016/S0012-821X(98)00033-8.

Muxworthy, A. R., D. J. Dunlop, and W. Williams (2003), High-temperature magnetic stability of small magnetite particles, *J. Geophys. Res.*, *108*(B5), 2281, doi:10.1029/2002JB002195.

Pike, C. R., A. P. Roberts, and K. L. Verosub (1999), Characterizing interactions in fine magnetic particle systems using first order reversal curves, *J. Appl. Phys.*, *85*, 6660–6667, doi:10.1063/1.370176.

Pike, C. R., A. P. Roberts, and K. L. Verosub (2001), First-order reversal curve diagrams and thermal relaxation effects in magnetic particles, *Geophys. J. Int.*, *145*, 721–730, doi:10.1046/j.0956-540x.2001.01419.x.

Reynolds, R. L., M. L. Tuttle, C. A. Rice, N. S. Fishman, J. A. Karachewski, and D. M. Sherman (1994), Magnetization and geochemistry of greigite-bearing Cretaceous strata, North Slope Basin, Alaska, *Am. J. Sci.*, *294*, 485–528.

Roberts, A. P. (1995), Magnetic characteristics of sedimentary greigite (Fe_3S_4), *Earth Planet. Sci. Lett.*, *134*, 227–236, doi:10.1016/0012-821X(95)00131-U.

Roberts, A. P., and G. M. Turner (1993), Diagenetic formation of ferrimagnetic iron sulphide minerals in rapidly deposited marine sediments, South Island, New Zealand, *Earth Planet. Sci. Lett.*, *115*, 257–273, doi:10.1016/0012-821X(93)90226-Y.

Roberts, A. P., Y. L. Cui, and K. L. Verosub (1995), Wasp-waisted hysteresis loops: Mineral magnetic characteristics and discrimination of components in mixed magnetic systems, *J. Geophys. Res.*, *100*, 17,909–17,924, doi:10.1029/95JB00672.

Roberts, A. P., R. L. Reynolds, K. L. Verosub, and D. P. Adam (1996), Environmental magnetic implications of greigite formation in a 3 m.y. lake sediment record from Butte Valley, northern California, *Geophys. Res. Lett.*, *23*, 2859–2862, doi:10.1029/96GL02831.

Roberts, A. P., C. R. Pike, and K. L. Verosub (2000), FORC diagrams: A new tool for characterizing the magnetic properties of natural samples, *J. Geophys. Res.*, *105*, 28,461–28,475, doi:10.1029/2000JB900326.

Roberts, A. P., Q. Liu, C. J. Rowan, L. Chang, C. Carvallo, J. Torrent, and C. S. Horng (2006), Characterization of

hematite (α-Fe_2O_3), goethite (α-FeOOH), greigite (Fe_3S_4), and pyrrhotite (Fe_7S_8) using first-order reversal curve diagrams, *J. Geophys. Res.*, *111*, B12S35, doi:10.1029/2006JB004715.

Ron, H., N. R. Nowaczyk, U. Frank, M. J. Schwab, R. Naumann, B. Striewski, and A. Agnon (2007), Greigite detected as dominating remanence carrier in late Pleistocene sediments, Lisan Formation, from Lake Kinneret (Sea of Galilee), Israel, *Geophys. J. Int.*, *170*, 117–131, doi:10.1111/j.1365-246X.2007.03425.x.

Rowan, C. J., and A. P. Roberts (2006), Magnetite dissolution, diachronous greigite formation, and secondary magnetizations from pyrite oxidation: Unravelling complex magnetizations in Neogene marine sediments from New Zealand, *Earth Planet. Sci. Lett.*, *241*, 119–137, doi:10.1016/j.epsl.2005.10.017.

Sagnotti, L., and A. Winkler (1999), Rock magnetism and palaeomagnetism of greigite-bearing mudstones in the Italian peninsula, *Earth Planet. Sci. Lett.*, *165*, 67–90, doi:10.1016/S0012-821X(98)00248-9.

Smirnov, A. V. (2006), Low-temperature magnetic properties of magnetite using first-order reversal curve analysis: Implications for the pseudo-single-domain state, *Geochem. Geophys. Geosyst.*, *7*, Q11011, doi:10.1029/2006GC001397.

Snowball, I. F. (1997a), Gyroremanent magnetization and the magnetic properties of greigite-bearing clays in southern Sweden, *Geophys. J. Int.*, *129*, 624–636, doi:10.1111/j.1365-246X.1997.tb04498.x.

Snowball, I. F. (1997b), The detection of single-domain greigite (Fe_3S_4) using rotational remanent magnetization (RRM) and the effective gyro field (B_g): Mineral magnetic and palaeomagnetic applications, *Geophys. J. Int.*, *130*, 704–716, doi:10.1111/j.1365-246X.1997.tb01865.x.

Snowball, I. F., and R. Thompson (1988), The occurrence of greigite in sediments from Loch Lomond, *J. Quat. Sci.*, *3*, 121–125, doi:10.1002/jqs.3390030203.

Snowball, I. F., and R. Thompson (1990), A stable chemical remanence in Holocene sediments, *J. Geophys. Res.*, *95*, 4471–4479, doi:10.1029/JB095iB04p04471.

Spender, M. R., J. M. D. Coey, and A. H. Morrish (1972), The magnetic properties and Mössbauer spectra of synthetic samples of Fe_3S_4, *Can. J. Phys.*, *50*, 2313–2326.

Tang, Y., Q. W. Chen, Y. Xiong, and Y. Li (2007), Magnetic field-induced increase in conversion rate of Fe_3S_4 to FeS_2, *Chin. J. Inorg. Chem.*, *23*, 941–947.

Torii, M., K. Fukuma, C. S. Horng, and T. Q. Lee (1996), Magnetic discrimination of pyrrhotite- and greigite-bearing sediment samples, *Geophys. Res. Lett.*, *23*, 1813–1816, doi:10.1029/96GL01626.

Tric, E., C. Laj, C. Jéhanno, J.-P. Valet, C. Kissel, A. Mazaud, and S. Iaccarino (1991), High-resolution record of the Upper Olduvai transition from Po Valley (Italy) sediments: Support for dipolar transition geometry?, *Phys. Earth Planet. Inter.*, *65*, 319–336, doi:10.1016/0031-9201(91)90138-8.

van Dongen, B. E., A. P. Roberts, S. Schouten, W. T. Jiang, F. Florindo, and R. D. Pancost (2007), Formation of iron sulfide nodules during anaerobic oxidation of methane, *Geochim. Cosmochim. Acta*, *71*, 5155–5167, doi:10.1016/j.gca.2007.08.019.

Vandenberghe, R. E., E. De Grave, P. M. A. De Bakker, M. Krs, and J. J. Hus (1991), Mössbauer effect study of natural greigite, *Hyperfine Interact.*, *68*, 319–322, doi:10.1007/BF02396500.

Vasiliev, I., M. J. Dekkers, W. Krijgsman, C. Franke, C. G. Langereis, and T. A. T. Mullender (2007), Early diagenetic greigite as a recorder of the palaeomagnetic signal in Miocene-Pliocene sedimentary rocks of the Carpathian foredeep (Romania), *Geophys. J. Int.*, *171*, 613–629.